

Precision YN and $\bar{n}N$ measurements with an LH_2/LD_2 target in the BESIII detector

Zhao-Ling Zhang,¹ Xu Gao,¹ Wei-Min Song,¹ and Chang-Zheng Yuan^{2,3}

¹*College of Physics, Jilin University, Changchun 130012, China*

²*Institute of High Energy Physics, Chinese Academy of Sciences, Beijing 100049, China*

³*University of Chinese Academy of Sciences, Beijing 100049, China*

(Dated: March 18, 2026)

Located at the BEPCII e^+e^- collider, the BESIII experiment provides a robust platform for investigating (anti)hyperon-nucleon (YN) and antineutron-nucleon ($\bar{n}N$) interactions. This is made possible by the high production cross-sections of J/ψ and $\psi(3686)$ resonances and their substantial decay branches into these baryons. Although previous studies using the beam pipe as a target demonstrated feasibility, statistical precision remains constrained by the limited material budget. To address this, we propose installing a dedicated liquid hydrogen or liquid deuterium target between the beam pipe and the Cylindrical Gas Electron Multiplier Inner Tracker. Monte Carlo simulations confirm that the added material has a negligible effect on charged particle tracking. This upgrade is expected to enhance the effective luminosity for scattering on free protons by a factor of 10–30 for Λ , Σ^+ , Ξ , and \bar{n} beams, enabling high-precision measurements of YN and $\bar{n}N$ interactions that will significantly advance our knowledge of non-perturbative strong interactions.

I. INTRODUCTION

The study of baryon-baryon and baryon-antibaryon interactions is fundamental to elucidating the strong interaction within the non-perturbative regime of quantum chromodynamics (QCD) and to probing the internal structure of baryons [1–6]. While scattering experiments constitute the most direct approach to investigating these dynamics, the short lifetimes of hyperons and the technical challenges associated with generating high-intensity antineutron beams have historically constrained experimental progress in this field.

Complementary to the nucleon-nucleon sector, (anti)hyperon-nucleon (YN) interactions introduce the strangeness degree of freedom, serving as a crucial probe for SU(3) flavor symmetry breaking and for understanding the role of hyperons in dense neutron star matter [7]. Describing baryon-baryon interactions within a unified model has always been a challenge in both particle and nuclear physics, but experimental data on YN scattering remain remarkably sparse. Historical measurements were primarily conducted during the bubble chamber era of the 1960s and 1970s [8–12], character-

ized by low statistics and large uncertainties. Recent measurements at J-PARC [13–15] and CLAS [16] have improved the situation, but further experimental data are imperative to improve precision and extend kinematic coverage.

In parallel, the antineutron-nucleon ($\bar{n}N$) system—and the antineutron-proton ($\bar{n}p$) channel in particular—offers a unique probe of nucleon-antinucleon dynamics. Unlike the proton-antiproton system, the $\bar{n}p$ channel is characterized by a pure isospin $I = 1$ state and the absence of Coulomb interference. Historically, antineutron beams were generated via the charge-exchange reaction $\bar{p}p \rightarrow \bar{n}n$, a method employed by experiments such as BNL E-767 [17] and CERN OBELIX [18]. These experiments provided essential data on antineutron interactions up to momenta of approximately 500 MeV/c [17, 19, 20], as well as contributions to meson spectroscopy [21, 22], but suffered from low conversion efficiency and limited beam intensities. Consequently, experimental data on antineutron interactions remain scarce, particularly in the momentum region exceeding 500 MeV/c.

To address these challenges, a novel approach has been proposed to produce antineutron and hyperon beams via J/ψ or $\psi(3686)$ decays at

electron-positron colliders [23, 24]. Taking advantage of the large resonance production cross-sections and significant branching fractions into baryons, this method delivers high-intensity beams with extended momentum coverage, extending well beyond the 500 MeV/ c limit of previous antineutron beam experiments. By fully reconstructing the recoil particles, the beam particles can be tagged, enabling precise measurements in the clean low-background environment of e^+e^- collisions. The BESIII Collaboration has successfully demonstrated the feasibility of this technique using the beam pipe as a target [25–29]; however, the physics potential of these studies was inherently constrained by the limited effective luminosity due to the thin material budget of the beam pipe. Furthermore, the composite nature of the beam pipe materials complicates the extraction of YN and $\bar{n}N$ cross sections, as nuclear structure effects introduce large systematic uncertainties into the results.

This work proposes the installation of a dedicated liquid hydrogen (LH₂) or liquid deuterium (LD₂) target positioned between the beam pipe and the Cylindrical Gas Electron Multiplier Inner Tracker (CGEM-IT) at BESIII. This upgrade aims to substantially boost the effective luminosity for YN and $\bar{n}N$ scattering experiments. Crucially, the use of LH₂ and LD₂ targets allows for direct extraction of the cross sections without complex nuclear-structure corrections, which is a significant advantage over the beam pipe material. Furthermore, the minimalist design of the target minimizes multiple scattering, thereby preserving the high-precision tracking performance of the BESIII detector.

II. TARGET DESIGN AND PROPERTIES

The BESIII detector [31] is a magnetic spectrometer operating at the BEPCII e^+e^- collider [32]. The detector consists of a multilayer drift chamber (MDC), a time-of-flight system (TOF), a CsI(Tl) electromagnetic calorimeter (EMC), and a muon chamber system (MUC)

incorporated into the return yoke of a superconducting solenoid magnet, which provides a 1.0 T magnetic field.

To extend the physics reach of the spectrometer toward the study of YN and $\bar{n}N$ interactions, a dedicated internal target system is proposed. Consisting of free protons, LH₂ is the ideal target for investigating Yp and $\bar{n}p$ interactions, providing direct access to cross sections uncomplicated by nuclear binding effects. Similarly, LD₂ serves as the premier proxy for neutron targets. While its nucleons (bound as deuterons) are not entirely free, LD₂ is preferred because it minimizes nuclear structure corrections relative to heavier nuclear targets. At their respective boiling points under atmospheric pressure, LH₂ (20.3 K) has a density of 0.071 g/cm³ and LD₂ (23.7 K) has a density of 0.164 g/cm³.

The proposed target, featuring a radial thickness of 40 mm, is positioned within the radial interval of 35–75 mm. This region lies in the gap between the beam pipe ($r = 33.7$ mm) and the CGEM-IT detector ($r = 76.9$ mm) [33]. The target consists of a double-walled cylindrical vessel constructed from thin Kapton film, with LH₂ or LD₂ filling the annular volume. Kapton was selected as the containment material since it satisfies all critical requirements: a low effective atomic number ($Z_{\text{eff}} \sim 5$) to limit electromagnetic background and multiple scattering, combined with high radiation resistance and mechanical robustness at ~ 20 K. Crucially, the use of Kapton for LH₂ containment is a well-established technique; similar designs have been successfully deployed in previous experiments, thereby strongly validating the feasibility of this approach [34].

Due to the short mean lifetimes of hyperons, these particles may decay before reaching or within the target region. To quantify this effect, we calculate the survival ratio N/N_0 of hyperons and antineutrons from the interaction point to the target region as a function of radial distance r after considering the detector acceptance, following the methodology described in Ref. [24]. The results are illustrated in Fig. 1, where N_0 represents the initial number of par-

ticles produced at the interaction point, while N denotes the number of particles that survive to a given radial distance r . As the survival probability depends on the particle momentum and angular distribution, the calculation is performed using representative production channels, which are summarized in Tab. I. For hyperons other than the Ω^- , we assume production via $J/\psi \rightarrow Y\bar{Y}$ decays; for the Ω^- , which is too massive to be produced in J/ψ decays, the process $\psi(3686) \rightarrow \Omega^-\bar{\Omega}^+$ is used. The production angular distributions for these hyperons are described by $1 + \alpha \cos^2 \theta$ [35, 36], with the parameter α determined from experimental measurements [37–43].

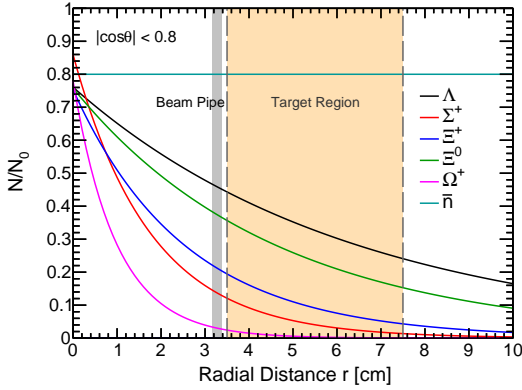


FIG. 1. Survival ratio N/N_0 of hyperons (Λ , Σ^+ , Ξ^0 , Ξ^-) and antineutrons (\bar{n}) from the interaction point to the target region as a function of radial distance r , with different particles indicated by different colored lines. The beam pipe and target regions are indicated by grey and yellow shaded areas, respectively. Considering the detector acceptance, particles with $|\cos \theta| > 0.8$ are rejected.

To assess the advantages of employing dedicated LH_2 and LD_2 targets over the existing beam pipe material for YN and $\bar{n}N$ scattering studies, we evaluate the areal number density \mathcal{T} for each target material as shown in Eq. 1. This quantity directly influences the effective luminosity for scattering experiments, as discussed in Section IV.

TABLE I. Decay modes, branching fractions, and momenta of hyperons and antineutrons from J/ψ and $\psi(3686)$ decays.

Baryon	Decay mode	BF ($\times 10^{-3}$)	P (MeV/c)
Λ	$J/\psi \rightarrow \Lambda\bar{\Lambda}$	1.89(9)	1074
Σ^+	$J/\psi \rightarrow \Sigma^+\bar{\Sigma}^-$	1.07(4)	992
Ξ^0	$J/\psi \rightarrow \Xi^0\bar{\Xi}^0$	1.17(4)	818
Ξ^-	$J/\psi \rightarrow \Xi^-\bar{\Xi}^+$	0.97(8)	807
Ω^-	$\psi(3686) \rightarrow \Omega^-\bar{\Omega}^+$	0.056(3)	774
\bar{n}	$J/\psi \rightarrow p\pi^-\bar{n}$	2.12(9)	0–1174

$$\mathcal{T} = \frac{\rho \cdot l}{M} \cdot N_A, \quad (1)$$

where ρ is the target density, l is the average path length of the incident beam inside the target, M is the molar mass and N_A is Avogadro's number.

Although \mathcal{T} is primarily determined by the target material properties (ρ and M), the average in-target path length l depends on the lifetimes of the incident particles and their angular distributions. Geometrically, particles with larger $|\cos \theta|$ traverse a longer distance through the cylindrical target shell compared to those traveling perpendicular to the beam axis; thus, the average path length is sensitive to the production angular distribution. Furthermore, for short-lived particles, l is effectively reduced by decays occurring before or during target traversal. In this work, we calculate l using the same production and decay channels utilized for the survival ratio estimation described in Fig. 1.

Unlike pure liquid targets, the beam pipe is a composite structure consisting of layers of Au, Be, and cooling oil [31]. Aside from the hydrogen in the oil, the nucleons in these materials are bound within nuclei. We thus estimate the areal number density \mathcal{T} for all protons, neutrons, and free protons (from the oil) within the beam pipe. To account for the effective interaction rates of bound nucleons, we employ the surface interaction model [19], assuming the effective cross section scales with $A^{2/3}$. Accordingly, the calculated \mathcal{T} is adjusted by scaling factors of $A^{2/3}(Z/A)$ for protons and $A^{2/3}((A-Z)/A)$ for

neutrons to normalize the interaction rates to the nucleon level. As shown in Table II, the LH₂ target provides a free-proton areal density 10–30 times greater than the beam pipe for most hyperon and antineutron beams. However, for the Ω^- hyperon, its short lifetime leads to substantial decay before reaching the target, limiting the gain to a factor of approximately 5.

TABLE II. Areal number density \mathcal{T} (in units of 10^{22} cm^{-2}) for the beam pipe (BP) and the proposed liquid targets, evaluated for each incident beam species. For the BP, the effective nucleon densities for neutrons (n) and total protons (p) are obtained by applying the $A^{2/3}$ nuclear scaling factor, while the free-proton (p_f) contribution arises solely from the hydrogen content of the cooling oil. For the LH₂ target, \mathcal{T} corresponds to free protons (p_f). For the LD₂ target, the neutron and proton densities are equal and denoted as n/p .

Beam	BP (\mathcal{T})			Target (\mathcal{T})	
	n	p	p_f	LH ₂ (p_f)	LD ₂ (n/p)
Λ	3.55	3.34	0.41	8.54	9.90
Σ^+	0.91	0.85	0.10	1.07	1.24
Ξ^-	1.64	1.54	0.19	2.55	2.95
Ξ^0	2.88	2.70	0.33	6.19	7.18
Ω^-	0.22	0.21	0.03	0.15	0.17
\bar{n}	5.85	5.50	0.68	19.60	22.70

III. IMPACT ON DETECTOR PERFORMANCE

The introduction of target material between the beam pipe and the CGEM-IT detector inevitably introduces multiple scattering and energy loss, which could potentially degrade the tracking efficiency and resolution of charged particles. Following the methodology established in Ref. [30], we evaluated these effects using a full Monte Carlo (MC) simulation with the updated BESIII detector geometry, which incorporates the CGEM-IT.

To systematically evaluate the dependence of the detector performance on the material

budget, simulations were performed for a baseline configuration (without any target material) as well as for both LH₂ and LD₂ targets at thicknesses of 20 and 40 mm. The target configurations specifically included the realistic modeling of the 0.1-mm-thick Kapton walls enclosing the cryogenic liquids. Protons, kaons, and pions—the primary stable charged particles in J/ψ decays—were generated to cover their respective kinematic regions of interest: 0.1–1.5 GeV/ c for pions, 0.2–1.5 GeV/ c for kaons, and 0.3–1.5 GeV/ c for protons. For each configuration, one million events were generated, evenly split between particles and antiparticles.

Key performance metrics, including detection efficiency (ϵ), momentum resolution (σ_p), and polar angle resolution (σ_θ), were determined using the σ_{68} method. This non-parametric approach, defined as the half-width of the 68.3% quantile interval of the residual distribution, ensures robustness against non-Gaussian tails. The relative changes in performance compared to the baseline configuration, expressed as $\Delta\epsilon/\epsilon_0$, $\Delta\sigma_p/\sigma_{p0}$, and $\Delta\sigma_\theta/\sigma_{\theta0}$ (where the subscript “0” represents the nominal values without the target), are summarized in Fig. 2.

The results demonstrate that the target material exerts minimal influence on the overall tracking performance. As shown in Fig. 2 (left), the efficiency ϵ decreases moderately with target thickness. The most noticeable reduction (approximately 7% for protons) occurs with the 40 mm LD₂ target, while the 20 mm LH₂ target exhibits a marginal loss of less than 2%. The degradation in σ_p and σ_θ is strictly controlled, remaining below 6% across all tested particle species. As expected, the LD₂ targets induce slightly larger broadening than LH₂ due to their higher material density. Overall, these studies indicate that even a 40 mm target induces only marginal performance loss, which is well within the tolerances required for the proposed physics program.

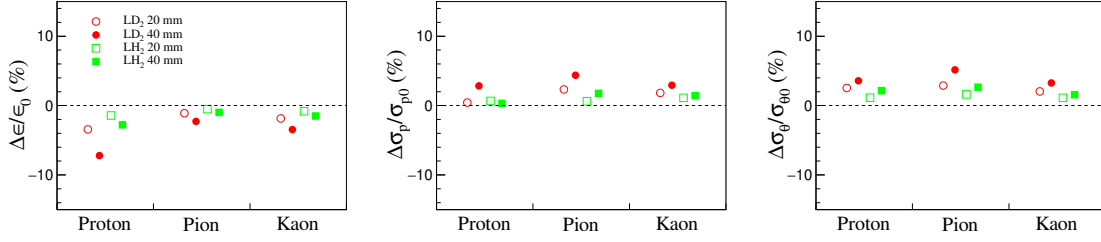


FIG. 2. Relative changes in (left) detection efficiency $\Delta\epsilon/\epsilon_0$, (middle) momentum resolution $\Delta\sigma_p/\sigma_{p0}$, and (right) polar angle resolution $\Delta\sigma_\theta/\sigma_{\theta0}$. Red circles and green squares represent LD₂ and LH₂, respectively; open and filled symbols denote target thicknesses of 20 mm and 40 mm.

IV. EXPECTED SIGNAL YIELDS

The procedure for estimating the signal yield is based on the approach used in studies of YN interactions at BESIII [23, 24]. Taking advantage of the clean e^+e^- collision environment, specific hyperons and antineutrons can be successfully tagged via their production in J/ψ and $\psi(3686)$ decays. Consequently, the reconstruction of scattering events is performed in two distinct steps: identifying the incident particle (the tagging side) and reconstructing the resulting scattering products (the signal side). Within this framework, the yield of the tagged incident particles can be expressed as:

$$N_{\text{tag}} = N_{\text{parent}} \cdot \mathcal{B}_{\text{tag}} \cdot \epsilon_{\text{tag}}, \quad (2)$$

where N_{parent} denotes the total number of J/ψ or $\psi(3686)$ particles. The factor \mathcal{B}_{tag} represents the branching fraction of the tagging channels, as summarized in Table I, and ϵ_{tag} is the tagging efficiency. Note that ϵ_{tag} intrinsically includes the branching fractions of the intermediate decay chains involved in the tag, such as $\mathcal{B}(\Lambda \rightarrow p\pi^-)$ for the Λ hyperon.

The effective luminosity of the incident particle beam, \mathcal{L}_Y , is determined by multiplying the number of tagged particles N_{tag} by the areal number density \mathcal{T} of the target. The expected yield of reconstructed scattering events, N_{obs} , can then be calculated using the formula:

$$N_{\text{obs}} = \mathcal{L}_Y \cdot \sigma \cdot \epsilon_{\text{sig}}, \quad (3)$$

where σ denotes the scattering cross section. The term ϵ_{sig} represents the reconstruction efficiency for the scattering products; similarly to ϵ_{tag} , it also includes the branching fractions of the final states used for reconstructing the scattering products. The target areal density, \mathcal{T} , is detailed in Section II.

As demonstrated by the preceding calculations, the expected signal yield is directly proportional to N_{parent} , the total number of produced J/ψ or $\psi(3686)$ events. We estimate the potential N_{parent} for a dedicated year of data taking (assuming 10 months of effective operation) based on historical BEPCII performance, factoring in an anticipated 30% luminosity improvement from the top-up injection scheme [44]. The most recent J/ψ data acquisition at BESIII, completed in 2019, yielded an integrated luminosity of 1200 pb^{-1} over 86 days. Given a J/ψ production cross section of approximately 3400 nb (accounting for the radiative correction and the energy spread of the collider), scaling this to 10 months of effective operation yields an expected sample of about 1.9×10^{10} J/ψ events. Similarly, extrapolating from the 2021 $\psi(3686)$ run, which accumulated 3350 pb^{-1} over 126 days with a production cross section of 640 nb, the expected number of $\psi(3686)$ events for a 10-month operational period is approximately 5.1×10^9 .

Based on these projections, we estimate the expected signal yields for a single dedicated year of data taking for the YN and $\bar{n}N$ scattering processes previously investigated at BESIII [25–

29]. Because the addition of the target material has a negligible impact on detector performance (as demonstrated in Section III), the efficiency parameters from corresponding BESIII analyses are adopted directly. The resulting estimated signal yields are summarized in Table III. Notably, the Ω^- hyperon is excluded from these projections. Its extremely short lifetime causes the vast majority of Ω^- particles to decay before reaching the target, yielding an expectation of only ~ 1 scattering events even under optimistic assumptions ($\sigma = 50$ mb, $\epsilon_{\text{tag}} \cdot \epsilon_{\text{sig}} = 5\%$). Consequently, it remains highly challenging to study Ω^- -nucleon scattering at BESIII.

Beyond the substantial gain in statistics, the proposed targets also offer a significant reduction in systematic uncertainties. The beam pipe is a composite structure containing Au, Be, and cooling oil, surrounded by additional components such as cooling pipes. While the hydrogen atoms in the cooling oil act as free protons and introduce no nuclear corrections, the nucleons in all other constituents are bound inside nuclei. Extracting nucleon-level cross sections from these heavy materials requires nuclear-model-dependent corrections, such as the $A^{2/3}$ surface-interaction scaling adopted in Section II, which introduce considerable systematic uncertainties. For example, in the BESIII measurement of $\Lambda + p \rightarrow \Sigma^+ + X$ [27], the total systematic uncertainty of 9.5% is dominated by contributions from the cooling pipe material (6.1%) and the nuclear scaling model (3.6%). By contrast, the pure LH₂ target consists entirely of free protons, eliminating nuclear corrections altogether and enabling a direct extraction of Yp and $\bar{n}p$ cross sections.

V. CONCLUSION AND DISCUSSION

In this work, we present a comprehensive feasibility study for the implementation of a dedicated LH₂ or LD₂ target system situated between the beam pipe and the CGEM-IT detector at the BESIII experiment. By capitalizing on the high production rates of J/ψ and $\psi(3686)$ resonances, the BESIII detector serves

as an ideal factory for hyperons and antineutrons. The clean e^+e^- collision environment enables the exclusive reconstruction of recoil particles, effectively mitigating background. These proposed targets will facilitate high-precision measurements of YN and $\bar{n}N$ interactions.

MC simulations demonstrate that the target material's impact on tracking efficiency and momentum resolution is negligible, particularly when weighed against the significant boost in event rates. Furthermore, replacing composite beam-pipe materials with pure LH₂ or LD₂ eliminates the substantial systematic uncertainties inherent in the nuclear modeling of complex materials such as beryllium.

Our estimates show that this configuration will enhance the effective luminosity for scattering on free protons by a factor of 10–30 for most hyperon and antineutron beams compared to the current beam pipe configuration. The only notable exception is the Ω^- hyperon, whose extremely short lifetime causes most particles to decay before reaching the target, resulting in a significantly smaller gain of approximately a factor of 5. Despite this limitation for the Ω^- , such a dramatic overall increase in statistical power will support a broad physics program, such as differential cross section measurements for YN interactions using three-body decays of J/ψ and $\psi(3686)$. Although the Ω^- -nucleon channel remains out of reach at BESIII, the technical framework established here provides a roadmap for future high-luminosity facilities such as STCF [45] and SCTF [46], where the expected luminosity increase of two orders of magnitude could make such measurements feasible.

It should be noted that while LH₂ and LD₂ are the ideal choices for extracting cross sections without nuclear structure complexities, their implementation poses significant technical challenges related to cryogenics and safety within the confined space of the BESIII detector. As a practical and more easily implementable alternative, room-temperature materials rich in hydrogen or deuterium, such as polyethylene (CH₂)_n, deuterated polyethylene (CD₂)_n, lithium hydride (LiH), or heavy wa-

TABLE III. Estimated signal yields for YN and $\bar{n}N$ scattering processes at BESIII. The columns $N_{\text{obs}}(\text{BP})$ and σ are taken from existing BESIII measurements using the beam pipe as target [25–29], where the two uncertainties on σ are statistical and systematic, respectively. The column $N_{\text{obs}}(\text{LH}_2/\text{LD}_2)$ gives the projected yields with the proposed targets. Processes involving proton (p_f/p) targets correspond to LH₂, while those involving neutron (n) targets correspond to LD₂.

Process	$N_{\text{obs}}(\text{BP})$	σ (mb)	$N_{\text{obs}}(\text{LH}_2/\text{LD}_2)$
$\Lambda + p_f \rightarrow \Lambda + p$	60.9 ± 7.8	$12.2 \pm 1.6 \pm 1.1$	$\sim 2,400$
$\bar{\Lambda} + p_f \rightarrow \bar{\Lambda} + p$	72.0 ± 8.5	$27.4 \pm 3.2 \pm 2.5$	$\sim 2,800$
$\Lambda + p \rightarrow \Sigma^+ + X$	795 ± 101	$19.3 \pm 2.4 \pm 1.8$	$\sim 3,900$
$\Sigma^+ + n \rightarrow \Lambda p$	77.6 ± 20.8	$45.2 \pm 12.1 \pm 7.2$	~ 200
$\Sigma^+ + n \rightarrow \Sigma^0 p$	48.6 ± 15.9	$29.8 \pm 9.7 \pm 6.9$	~ 120
$\Xi^0 + n \rightarrow \Xi^- + p$	22.9 ± 5.5	$22.1 \pm 5.3 \pm 4.5$	~ 110
$\bar{n} + p_f \rightarrow 2\pi^+\pi^-$	59.0 ± 7.7	$2.7 \pm 0.3 \pm 0.3$	$\sim 3,200$
$\bar{n} + p_f \rightarrow 2\pi^+\pi^-\pi^0$	182.0 ± 13.5	$10.8 \pm 0.8 \pm 0.9$	$\sim 10,000$
$\bar{n} + p_f \rightarrow 2\pi^+\pi^-2\pi^0$	97.7 ± 10.0	$12.6 \pm 1.3 \pm 1.0$	$\sim 5,400$

ter (D₂O), could be employed. These materials actually provide a more compact source of target nucleons: the hydrogen volumetric number density in solid (CH₂)_n and LiH is approximately 1.9 and 1.4 times higher than that of LH₂, respectively. Similarly, the deuterium number density in solid (CD₂)_n and liquid D₂O is about 1.7 and 1.4 times higher than that of LD₂. While using such composite materials would reintroduce some nuclear corrections and decrease detector performance due to the presence of heavier elements like carbon or oxygen, they are highly cost-effective, offer enhanced effective luminosity per unit volume, and involve no cryogenic complications.

In summary, introducing a dedicated target system into the BESIII detector is both a conceptually innovative and practically feasible upgrade. Whether proceeding with the ideal cryogenic liquids or the highly efficient room-

temperature alternatives, this endeavor exploits the unique advantages of the BESIII J/ψ and $\psi(3686)$ data sets. By effectively converting an e^+e^- collider into a precision hyperon and antineutron factory, this proposed program will deliver irreplaceable inputs for QCD phenomenological models and mark a significant milestone in our exploration of the strong interaction.

ACKNOWLEDGMENTS

This work is supported in part by the National Natural Science Foundation of China under contract No. 12361141819 and the Program of Science and Technology Development Plan of Jilin Province of China under contract No. 20230101021JC.

[1] E. Epelbaum, H. W. Hammer and U. G. Meißner, *Rev. Mod. Phys.* **81**, 1773 (2009).

[2] R. Machleidt and D. R. Entem, *Phys. Rept.* **503**, 1 (2011).

- [3] S. K. Bogner, R. J. Furnstahl and A. Schwenk, *Prog. Part. Nucl. Phys.* **65**, 94 (2010).
- [4] E. Klempt *et al.*, *Phys. Rept.* **368**, 119 (2002).
- [5] T. Bressani and A. Filippi, *Phys. Rept.* **383**, 213 (2003).
- [6] A. Gal, E. V. Hungerford and D. J. Millener, *Rev. Mod. Phys.* **88**, 035004 (2016).
- [7] L. Tolos and L. Fabbietti, *Prog. Part. Nucl. Phys.* **112**, 103770 (2020).
- [8] G. Alexander *et al.*, *Phys. Rev.* **173**, 1452 (1968).
- [9] B. Sechi-Zorn *et al.*, *Phys. Rev.* **175**, 1735 (1968).
- [10] J. A. Kadyk *et al.*, *Nucl. Phys. B* **27**, 13 (1971).
- [11] F. Eisele *et al.*, *Phys. Lett. B* **37**, 204 (1971).
- [12] J. M. Hauptman, J. A. Kadyk and G. H. Trilling, *Nucl. Phys. B* **125**, 29 (1977).
- [13] K. Miwa *et al.* (J-PARC E40 Collaboration), *Phys. Rev. Lett.* **128**, 072501 (2022).
- [14] K. Miwa *et al.* (J-PARC E40 Collaboration), *Phys. Rev. C* **104**, 045204 (2021).
- [15] T. Nanamura *et al.* (J-PARC E40 Collaboration), *PTEP* **2022**, 093D01 (2022).
- [16] J. Rowley *et al.* (CLAS Collaboration), *Phys. Rev. Lett.* **127**, 272303 (2021).
- [17] T. Armstrong *et al.* (BNL-E-0767 Collaboration), *Phys. Rev. D* **36**, 659 (1987).
- [18] M. Agnello *et al.*, *Nucl. Instrum. Meth. A* **399**, 11 (1997).
- [19] M. Astrua *et al.*, *Nucl. Phys. A* **697**, 209 (2002).
- [20] F. Iazzi *et al.* (OBELIX Collaboration), *Phys. Lett. B* **475**, 378 (2000).
- [21] A. Bertin *et al.* (OBELIX Collaboration), *Phys. Rev. D* **57**, 55 (1998).
- [22] V. G. Ableev *et al.* (OBELIX Collaboration), *Phys. Lett. B* **334**, 237 (1994).
- [23] C. Z. Yuan and M. Karliner, *Phys. Rev. Lett.* **127**, 012003 (2021).
- [24] J. Dai, H. B. Li, H. Miao and J. Zhang, *Chin. Phys. C* **48**, 073003 (2024).
- [25] M. Ablikim *et al.* (BESIII Collaboration), [arXiv:2511.21462](https://arxiv.org/abs/2511.21462).
- [26] M. Ablikim *et al.* (BESIII Collaboration), *Phys. Rev. Lett.* **130**, 251902 (2023).
- [27] M. Ablikim *et al.* (BESIII Collaboration), *Phys. Rev. C* **109**, L052201 (2024).
- [28] M. Ablikim *et al.* (BESIII Collaboration), *Phys. Rev. Lett.* **132**, 231902 (2024).
- [29] M. Ablikim *et al.* (BESIII Collaboration), [arXiv:2505.19907](https://arxiv.org/abs/2505.19907).
- [30] S. Yuan, L. Wang and W. Li, *Radiat. Detect. Technol. Methods* **8**, 1405 (2024).
- [31] M. Ablikim *et al.* (BESIII Collaboration), *Nucl. Instrum. Meth. A* **614**, 345 (2010).
- [32] C. Yu *et al.*, *TUYA01* (2016).
- [33] I. Balossino *et al.*, *Symmetry* **14**, 905 (2022).
- [34] P. Roy *et al.*, *Nucl. Instrum. Meth. A* **949**, 162874 (2020).
- [35] G. Fäldt and A. Kupsc, *Phys. Lett. B* **772**, 16 (2017).
- [36] E. Perotti *et al.*, *Phys. Rev. D* **99**, 056008 (2019).
- [37] M. Ablikim *et al.* (BESIII Collaboration), *Phys. Rev. Lett.* **129**, 131801 (2022).
- [38] M. Ablikim *et al.* (BESIII Collaboration), *Nature* **606**, 64 (2022).
- [39] M. Ablikim *et al.* (BESIII Collaboration), *Phys. Rev. Lett.* **125**, 052004 (2020).
- [40] M. Ablikim *et al.* (BESIII Collaboration), *Nature Phys.* **15**, 631 (2019).
- [41] M. Ablikim *et al.* (BESIII Collaboration), *Phys. Rev. D* **106**, L091101 (2022).
- [42] M. Ablikim *et al.* (BESIII Collaboration), *Phys. Rev. D* **108**, L031106 (2023).
- [43] M. Ablikim *et al.* (BESIII Collaboration), *Phys. Rev. Lett.* **126**, 092002 (2021).
- [44] M. Ablikim *et al.* (BESIII Collaboration), *Chin. Phys. C* **44**, 040001 (2020).
- [45] M. Achasov *et al.*, *Front. Phys. (Beijing)* **19**, 14701 (2024).
- [46] A. E. Bondar *et al.* (Charm-Tau Factory Collaboration), *Phys. At. Nucl.* **76**, 1072 (2013).